Progress In Electromagnetics Research C, Vol. 81, 11–19, 2018

SRR-Loaded Metamaterial-Inspired Electrically-Small Monopole Antenna

Divya Chaturvedi* and Singaravelu Raghavan

Abstract—In this paper, a CPW-fed compact metamaterial-inspired monopole antenna is proposed for Industrial, Scientific and Medical radio band (ISM, 2.4–2.483 GHz). The proposed antenna consists of a T-shaped patch and a set of split ring resonators (SRRs). The miniaturization is attained after loading SRRs in proximity to the T-shaped radiator, which makes the antenna structure electrically small. The measured fractional bandwidth of the antenna is 4% (2.42–2.52 GHz), and its size is $0.22\lambda_o$ $0.098\lambda_o \times .013\lambda_o$. In addition, the electrically equivalent circuit of the proposed antenna is modeled, and the resonant frequency is calculated by using an analytical approach. Also, the permeability plot of SRRs is extracted using Nicolson Ross weir method. The measured peak gain and radiation efficiency of the antenna are obtained as 1.76 dBi and 78.5%. The simulated results and measured results are found in a good agreement.

1. INTRODUCTION

In a modern wireless communication system, with the development of portable electronic equipment, the size of the antenna has become a primary concern for accommodating in a limited space. In this regard, electrically small antennas (ESA) have potential and attractive features to fulfill the requirements of modern wireless communication systems. These types of antennas have gained tremendous attention due to their highly compact size, low profile and moderate bandwidth. In 1940's Chu [1] and Wheeler [2] developed an electrically small antenna (ESA) and derived the relationship between the size and bandwidth of the antenna. A plethora of ESA designs have been developed by using different techniques, where resonant and non-resonant based metamaterial inspired ESAs have attracted great attention. The fundamental principle to design ESA is that the maximum dimension of the antenna should fit inside the imaginary sphere of radius $\lambda_o/2\pi$,and it can be defined more explicitly by the relationship $k \times a < 1$, where 'a' is the radius of the imaginary sphere enclosing maximum dimensions of the antenna [3–5]. The challenge in designing ESA is the large impedance mismatch due to low radiation resistance, hence external matching network is used to receive the maximum input power level [6].

Metamaterial-inspired monopole antennas are good alternatives to overcome the limitation of the matching network. Moreover, these types of antennas satisfy all the properties of ESA. Metamaterial structure is a sub-wavelength resonator, which contains exciting properties to develop single negative (SNG) and double negative (DNG) materials [7]. Owing to the attractive features of coplanar waveguide (CPW) feed such as wider bandwidth, less dispersion CPW-fed metamaterial antennas have been used extensively [8, 9]. In the past decade, various techniques have been proposed to reduce the size of the antenna, using meandering the patch [10, 11], by loading a slot loop antenna with periodic capacitors to increase the propagation constant [12]. Several types of metamaterial geometries such as SRR, CSRR, spiral, OSRR are developed to realize MNG and ENG types of structures. These structures show some

Received 12 October 2017, Accepted 15 January 2018, Scheduled 25 January 2018
* Corresponding author: Divya Chaturvedi (divyanitt31@gmail.com).
The authors are with the Department of Electronics and Communication Engineering, National Institute of Technology, Tiruchirappalli 620 015, India.

unusual properties which are the reverse of the basic properties existing in the conventional type of materials. The SRR rings containing splits in the opposite or same side are one of the acknowledged elements to generate the negative value of permeability, known as mu-negative (MNG) metamaterial. An electrically small antenna is designed [13] by loading the patch with split ring resonators, but the thickness of the substrate is large, which makes it incompatible in integration with other devices. Non-resonant metamaterial antennas implemented with Composite Right/Left (CRLH) transmission line are reported in [14–16]. Metamaterial inspired structures are developed to generate multiple frequency bands [17–20].

In this work, a compact SRRs loaded antenna is designed to operate at 2.45 GHz. To verify the metamaterial properties, permeability plot is extracted by deploying Nicolson Ross Weir (NRW) method, and it shows the stopband at the resonant frequency of SRRs. The proposed antenna is modeled in terms of RLC equivalent circuit, and the resonant frequency is calculated as well as compared with the frequency obtained from full-wave simulations. The organization of the paper is summarized as follows. Section 2 presents antenna design, extraction of negative permeability and design of the electrical equivalent circuit. Section 3 presents the results and discussion of parameters.

2. ANTENNA DESIGN METHODOLOGY

The geometry of the proposed electrically small monopole antenna, which consists of a T-shaped patch and a set of rectangular SRR rings, is depicted in Fig. 1. A two-step evolution leads to a compact size antenna. In the first step, the antenna is designed with a T-shaped patch, which consists of two perpendicular strips and operates at 2.64 GHz. The length of the T-shaped patch is '$l_p + W$' $\sim \lambda_o/4$, satisfying the criteria of monopole antenna. The width of the feed is calculated as $0.041\lambda_\varepsilon$ to achieve characteristic impedance of 50 Ω. The antenna is fed at point A, and total length of the patch ($l_p + W$) is used to excite the dominant mode at 2.64 GHz. Impedance matching is critical in optimization for operating frequency band. Since the capacitive reactance is high, hence impedance variation is also high. The length and width of the first strip of the patch $l_p = 0.27\lambda_\varepsilon$, $w_t = 0.01\lambda_\varepsilon$ is used to match the 50 Ω impedance from feed to the second strip of the patch. A tapering section is used between feed and first strip of the patch to avoid losses due to reflection from sharp corners. In the second step, when the patch is loaded with rectangular SRR rings, the resonant frequency shifts to 2.45 GHz, shown in Fig. 2.

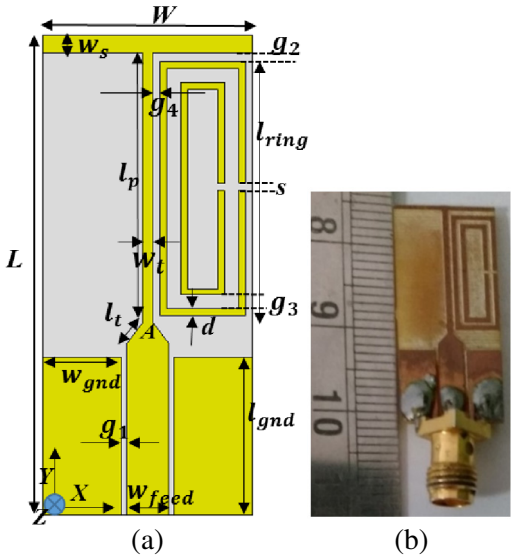

Figure 1. (a) Configuration of the proposed SRR-loaded antenna. (b) Fabricated prototype of the proposed antenna. Dimensions are specified in mm $L = 27.4$, $W = 12$, $w_s = 1$, $w_{feed} = 2.4$, $w_{gnd} = 4.5$, $l_{gnd} = 9$, $w_t = 0.6$, $l_p = 15.4$, $l_t = 1.5$, $g_1 = 0.3$, $g_2 = 0.5$, $g_3 = 0.8$, $g_4 = 0.4$, $s = 0.5$, $d = 0.4$, $l_{ring} = 14.4$.

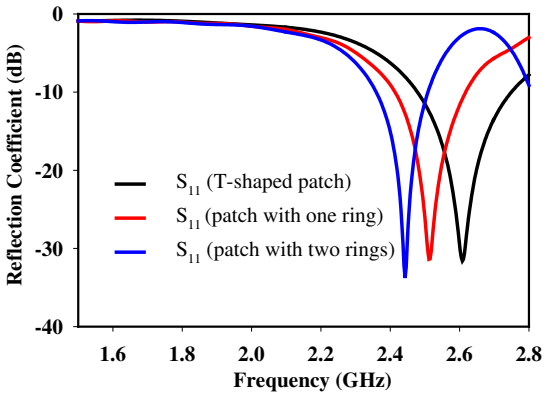

Figure 2. Simulated $|S_{11}|$ of proposed geometry with the loading of rectangular SRR rings.

When the rings are placed at a gap of 0.4 mm from the T-shaped patch, an electric field is induced in the SRR rings through the magnetic coupling from the patch. The excited SRR rings generates magnetic resonance phenomena, which introduces negative permeability at the resonance frequency of ring resonators. By loading the patch with SRR rings, the extra series and shunt inductance as well as capacitance are added in the circuit. In order to enhance the magnetic flux intensity, both rings are split in the same side and placed at a gap of 0.8 mm between the rings.

The miniaturization is achieved due to the phenomena of increment in the patch surface current path, because of increases in the overall inductance and capacitance from rings, which makes the proposed antenna electrically small. The antenna is fabricated on an inexpensive FR4 substrate with dielectric constant and loss tangent ($\varepsilon_r = 4.4$, $\tan\delta = 0.025$) and thickness of the filling substrate of 1.6 mm [8, 12]. The size of the proposed antenna is $0.45\lambda_\varepsilon \times 0.2\lambda_\varepsilon \times 0.027\lambda_\varepsilon$ (where λ_ε is the guiding wavelength at operating frequency of 2.45 GHz). The proposed antenna is simulated by using the Finite-Difference Time-Domain (FDTD) method based CST Microwave studio simulation solver. Split ring resonators can be categorized as mu-negative (MNG) type of material, hence the characterization of material is synthesized and explained in Subsection 2.1.

2.1. Permeability Plot Analysis

The quasi-static equivalent-circuit model of the SRR rings is plotted in Fig. 3. The resonant frequency is calculated from the equivalent inductance and capacitance of SRR rings by applying Equations (1)–(5) [21]. The equivalent inductance directly depends on the length of rings, the width of the rings and filling ratio

$$L_{SRR} = \frac{\mu_0}{2}\frac{l_{savg}}{4}4.86\left(\ln\frac{0.98}{\rho}+1.84\rho\right) \tag{1}$$

where μ_0 is the permeability of free space ($4\pi \times 10^{-7}$).

Filling ratio can be stated as

$$\rho = \left[\frac{(N-1)(d+g_3)}{[l_{ring}-(N-1)(d+g_3)]}\right] \tag{2}$$

Average length of the rings can be calculated as $l_{savg} = 4[l_{ring} - (N-1)(d+g_3)]$. N denotes the number of rings, d the width of rings, l_{ring} the length of the outer ring, and g_3 the gap between both rings.

Equivalent capacitance is calculated using the formula shown in Equation (3)

$$C_{SRR} = \frac{N-1}{2}\left[2l_{ring} - (2N-1)(d+g_3)\right]C_o \tag{3}$$

ε_0 is the dielectric constant in the air, k i the complete elliptic integral of the first kind, and

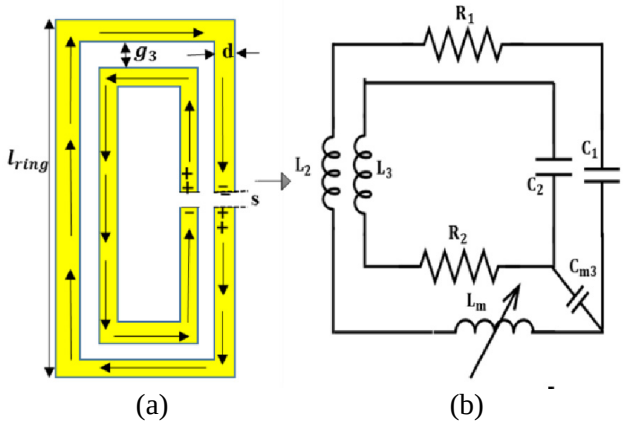

Figure 3. (a) Split ring resonators. (b) Equivalent-circuit model of SRR rings.

$k_1 = [g_3/2/(d + g_3/2)]$

$$C_o = \varepsilon_{ro}\varepsilon_r\,(h, d, g_3)\,\frac{K\sqrt{(1-k_1^2)}}{K(k_1)} \tag{4}$$

The equivalent inductance of the rings does not depend upon the thickness of the substrate but depends upon only the dimension of the rings and the number of rings. For an MNG resonator, resonant frequency is calculated from equation shown below

$$f_r = \frac{1}{2\pi\sqrt{L_{SRR}C_{SRR}}} \tag{5}$$

From the above defined equations, equivalent inductance and capacitance are calculated as $L_{SRR} = 0.11\,\mu\text{H}$ and $C_{SRR} = 0.3\,\text{pF}$. The resonant frequency of SRR rings is calculated from Equation (5) [13] which is 0.85 GHz. To analyze the relative permeability at resonant frequency, NRW method is implemented and described by using Equation (6). A waveguide setup shown in Fig. 4 is used to retrieve scattering parameters of the SRR single unit cell based on the classical waveguide theory [17]. In this waveguide setup, perfect electric conductor (PEC) boundary is applied along the X-axis (YZ-plane), and perfect magnetic conductor (PMC) boundaries are applied along the Z-axis (XY-plane), which is parallel to the plane of the rings. Electromagnetic waves are applied at port-1 and received at port-2. When the EM wave is excited from port-1, it is perturbed by the SRR rings, and a potential difference is generated in the split of the rings, shown in Fig. 3(a). Hence, displacement currents start to flow in opposite directions in both the rings. The split capacitance prevents the current from flowing while the gap capacitance between the rings forces the current to flow.

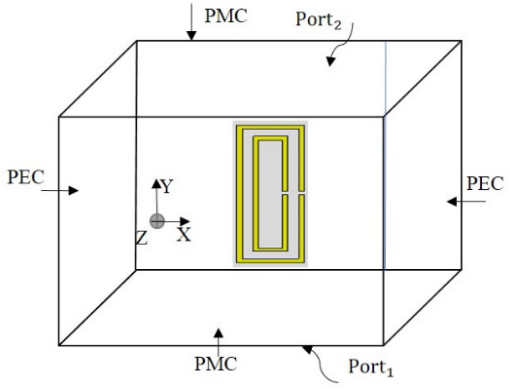

Figure 4. Simulation setup box for the rectangular SRR rings.

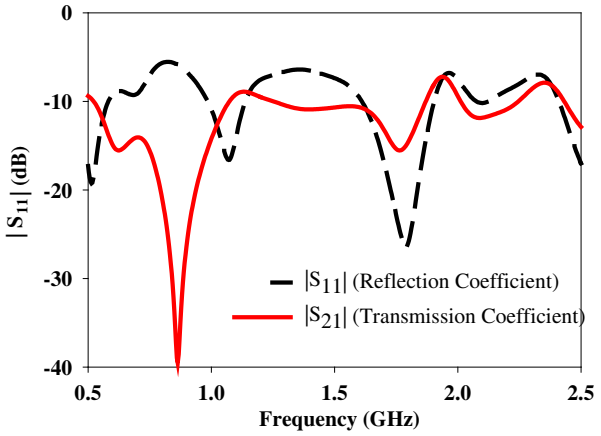

Figure 5. Extracted reflection and transmission coefficient parameters from waveguide set-up.

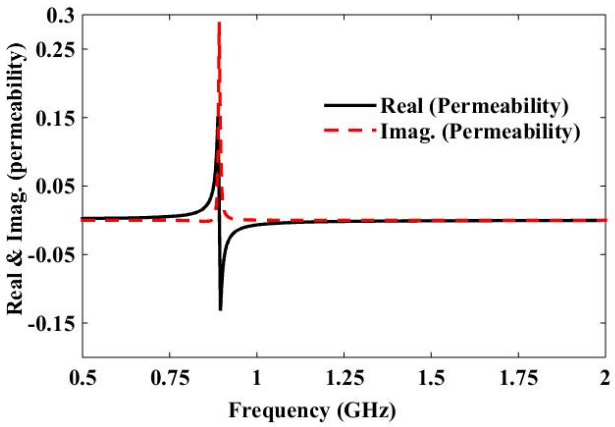

Figure 6. Permeability vs frequency plot.

Therefore, same magnitude current flows with a 180° phase difference in both the rings. The reflection and transmission coefficients are retrieved from the waveguide setup and plotted in Fig. 5. The reflection and transmission coefficients shows a stopband characteristic at 0.85 GHz. In the next process to extract the real and imaginary values of permeability, Nicolson Ross weir (NRW) method is used [17]. The extracted values of $|S_{11}|$ and $|S_{22}|$ are plotted in Fig. 6 with the help of MATLAB solver using Equation (6). A transition in the real value of permeability plot is observed in the frequency range of $0.75 \sim 1$ GHz, which exhibits a strong magnetic polarizability near its resonance and negative value of permeability at 0.85 GHz. This suggests that SRR is a single negative material and stops the waves to pass at the resonant frequency of SRR due to the presence of imaginary value of refractive index.

$$\mu_r = \frac{2}{jk_o h}\left(\frac{1-V_1}{1+V_1}\right) \tag{6}$$

where $V_1 = S_{22}+S_{11}$, and V_1 can be calculated from S-parameters. k_o is the wave number, and h is the thickness of substrate. In order to observe the effect of loading of SRR rings nearby patch, we have modeled the electrically equivalent RLC circuit of the proposed antenna. The series and shunt lumped elements are calculated with the analytical approach to determine the resonant frequency, described in Subsection 2.2.

2.2. Modeling of Electrical Equivalent Circuit

The equivalent RLC circuit of the proposed antenna is modeled in Fig. 7. The inductance and capacitance values of the passive elements are calculated from the dimensions of the patch numerically. The T-shaped patch consists of two strips, which are equivalent to the series combination of inductance L_1 and L_2, where L_1 is the inductance of the first strip, which is in series with another perpendicular strip of inductance L_2. The gaps between SRR rings and the patch are equivalent to series capacitances C_{m1} and C_{m2}. A shunt capacitance exists between the rings and the ground plane, represented by C_{m4}. A mutual capacitance C_{m3} which exists in gaps of both rings generates low capacitance value due to large gap, but the series capacitances C_{m1} and C_{m2} incorporate higher values than mutual and shunt capacitance [14].

The losses in the ring are incorporated by resistance R_1 and R_2 of both rings. The values of circuit parameters L, C from model are calculated as $L_1 = 13.5$ nH, $L_2 = 8.79$ nH, $C_{m1} = 9.86$ pF, $C_{m2} = 5.8$ pF, $L_{eq} = 42.8$ nH, $C_{eq} = 0.15$ pF [21]. By using mathematical approach, based on the series and shunt configuration, all the elements are solved, and the resonant frequency is obtained at 2.15 GHz [21]. The resonant frequency of the equivalent circuit model is obtained lower than the resonant frequency of the proposed antenna from full-wave simulation of 2.44 GHz. This discrepancy is due to neglecting of some lumped elements, where the resistances of rings are not involved in the calculation of the resonant frequency of equivalent circuit model. Hence, the losses due to patch resistance are

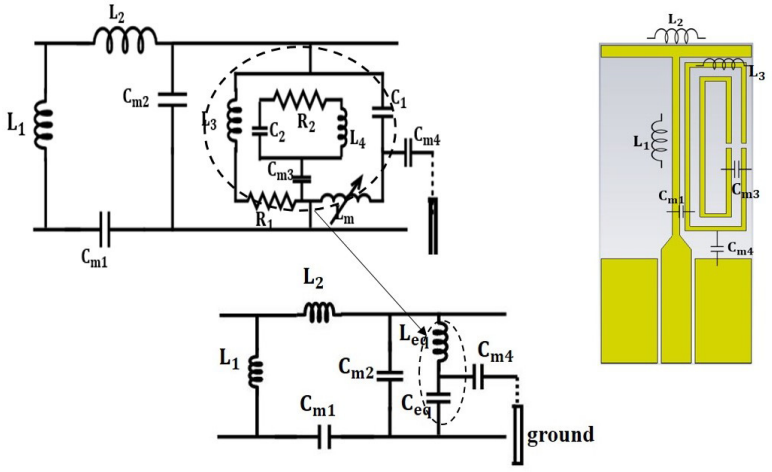

Figure 7. Electrical equivalent circuit of the proposed antenna.

neglected in calculating the resonant frequency. The analytical approach based resonant frequency and simulated resonant frequency are in good approximation. Chu proposed a relation to fundamental limits of radiation quality factor with an electrically small antenna, which is represented in [1–4]. Later, McLean proposed a more exact evaluation approach of radiation quality factor [5]. The proposed antenna can be categorized as an electrically small antenna by determining the Chu limit $k \times a$, where a is the smallest radius of the sphere containing the antenna, and k is the wave number. The value of Chu limit is $k \times a = \frac{2\pi}{\lambda} \times a = 0.744 < 1$ [2, 3], which confirms that the proposed antenna satisfies the condition of an electrically small antenna.

3. RESULTS AND DISCUSSION

The antenna is fabricated using a copper etching process and measured using Agilent E5071B (ENA Series) Network Analyzer [17]. In this section, parametric analysis and optimization are depicted. In Fig. 8, the variation of frequency by changing the patch strip width w_t is illustrated. The resonant frequency is shifted upward by increasing the width 'w_t' of the first strip of the patch. If the patch width increases, series inductance decreases, which suggests shifts of resonant frequency downward.

The perpendicular strip of the patch is deployed for impedance matching, hence as width decreases input impedance increases, and a better impedance matching is obtained at $w_t = 1.2\,\text{mm}$. In Fig. 9, the variation of frequency with respect to patch width 'w_s' is shown. If patch width decreases, the gap

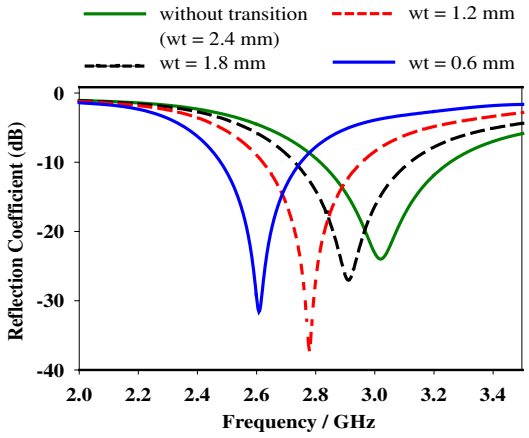

Figure 8. $|S_{11}|$ against frequency for different values of 'w_t' parameter.

between patch and ring increases, resulting in decrease in the coupling capacitance 'C_{m2}'; therefore, frequency shifts upward. The ground length also affects the resonant frequency, due to the existence of shunt capacitance 'C_{m4}', in the gap between rings and the ground plane, shown in Fig. 9. If the ground length increases, the mutual capacitance 'C_{m4}' increases, which results in shift of the frequency towards the lower side and provides miniaturization.

The simulated and measured return loss plots are displayed in Fig. 10. For the measured result, a slight upward shift of the resonant frequency and 1.6% reduction in the impedance bandwidth are noticed. This slight discrepancy might possibly exist due to fabrication tolerances and fabrication inaccuracies. To confirm the radiation properties, normalized simulated and measured radiation pattern plots are shown in Fig. 11 at ($\phi = 0°$) H-plane and ($\phi = 90°$) E-plane for the simulated resonant frequency at 2.45 GHz and measured resonant frequency at 2.47 GHz. The H-plane shows omnidirectional radiation pattern like a dipole, and the E-plane shows an eight-shaped type pattern. The simulated and measured results in the XZ-plane and YZ-plane are in good agreement. The measured peak gain of 1.76 dBi in the far-field radiation pattern is achieved along with radiation efficiency of 78.5%. The simulated cross-polarization level is lower by 20 dBi compared to co-polarized level in both planes. A comparison of parameters of simulation and measurement results is depicted in Table 1.

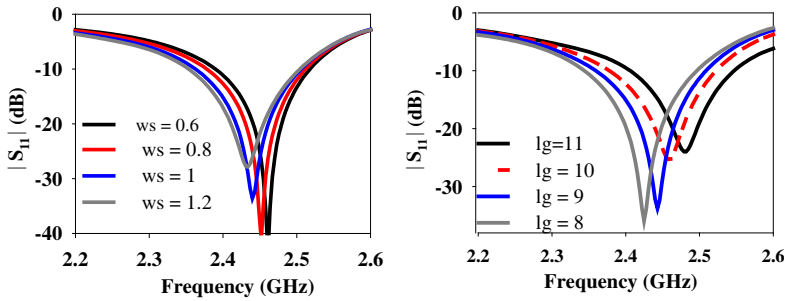

Figure 9. $|S_{11}|$ against frequency for different 'w_s' parameter, $|S_{11}|$ against frequency for different 'l_g' parameter.

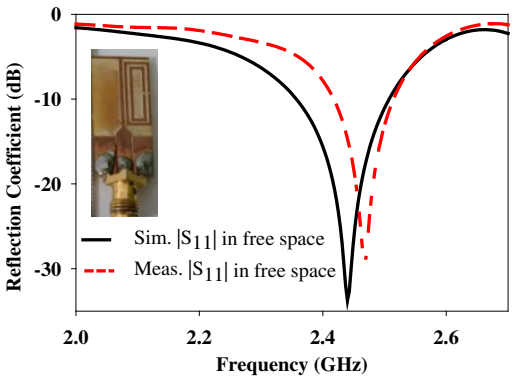

Figure 10. Comparison of Simulated and measured $|S_{11}|$ parameters.

Table 1. Comparison of simulated and measured results.

Parameters	Simulated results	Measured Result
Resonant Freq. (f_r)	2.45	2.47
Bandwidth (MHz)	140	100
Gain (dBi)	1.92	1.76
Efficiency (%)	87.6	78.5

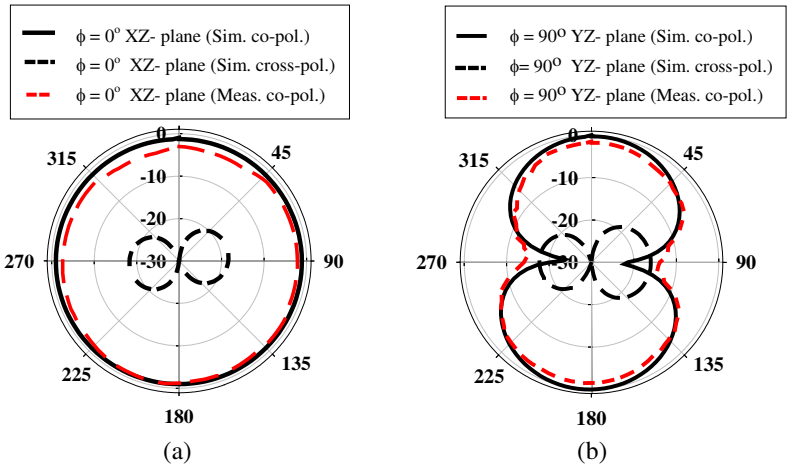

Figure 11. 2-D radiation pattern plots of E-plane ($\phi = 90°$) and H-plane ($\phi = 0°$). (a) Simulated co-pol., simulated cross-pol, and measured co-pol. radiation pattern plot in H-plane. (b) Simulated co-pol., simulated cross-pol, and measured co-pol. radiation pattern plot in E-plane.

4. CONCLUSION

In this paper, a compact SRR loaded electrically small monopole antenna has been presented, and the miniaturization is realized by loading split ring resonators. Single negative metamaterial property of SRR resonator has been extracted and confirmed that the proposed structure is inspired by the mu-negative material. The resonant frequency of the RLC electric equivalent circuit of the proposed antenna and from the full wave simulations is obtained in a good approximation. The realized parameters assure that the proposed ESA is a suitable and potential candidate for ISM band application.

REFERENCES

1. Chu, L. J., "Physical limitations of omni-directional antennas," *J. Appl. Phys.*, Vol. 19, No. 12, 1163–1175, 1948.
2. Wheeler, H. A., "Fundamental limitations of small antennas," *IRE Proceedings*, Vol. 35, l479–1484, 1947.
3. Ziolkowski, R. W. and A. Erentok, "At and below the Chu limit: passive and active broad bandwidth metamaterial-based electrically small antennas," *IET Microwaves Antennas Propag.*, Vol. 1, No. 1, 116–128, 2007.
4. Balanis, C. A., *Antenna Theory Analysis and Design*, 637–641, ISBN: 0-471-66782-X, John Wiley & Sons, New York, 2005,
5. Mclean, J. S., "A re-examination of the fundamental limits on the radiation Q of electrically small antennas," *IEEE Trans. Antennas Propag.*, Vol. 44, No. 5, 672–676, 1996.
6. Best, S. R., "Electrically small resonant planar antennas: optimizing the quality factor and bandwidth," *IEEE Antennas Propag. Mag.*, Vol. 57, No. 3, 38–47, 2015.
7. Caloz, C. and T. Itoh, *Electromagnetic Metamaterials: Transmission Line Theory and Microwave Applications*, ISBN: 9780471669852, John Wiley & Sons, 2005.
8. Si, L. M., W. Zhu, and H. J. Sun "A compact, planar, and CPW-fed metamaterial-inspired dual-band antenna," *IEEE Antennas Wirel. Propag. Lett.*, Vol. 12, 305–308, 2013.
9. Li, Y. and Q. Feng, "A compact tri-band monopole antenna with metamaterial loaded for WLAN/WiMAX applications," *Journal of Electromagnetic Waves and Applications*, Vol. 27, No. 6, 772–782, 2013.

10. Psychoudakis, D. and L. V. John, "Conformal asymmetric meandered flare (AMF) *antenna* for body-worn applications," *IEEE Antennas Wirel. Propag. Lett.*, Vol. 8, 931–934, 2009.
11. Wang, P., G. J. Wen, Y.J. Huang, and Y. H. Sun, "Compact meander T-shaped monopole antenna for dual-band WLAN applications," *Int. J. RF Microw. C.E.*, Vol. 23, No. 1, 67–73, 2013.
12. Chi, P. L., K. M. Leong, R. Waterhouse, and T. Itoh, "A miniaturized CPW-fed capacitor-loaded slot-loop antenna," *IEEE International Symposium on Signals (ISSSE'07)*, 595–598, 2007.
13. Joshi, J. G., S. S. Pattnaik, S. Devi, and M. R. Lohokare, "Electrically small patch antenna loaded with metamaterial," *IETE J. Res.*, Vol. 56, No. 6, 373-9, 2014.
14. Gonghan, W. and F. Quanyuan, "A novel coplanar waveguide feed zeroth-order resonant antenna with resonant ring," *IEEE Antennas Wirel. Propag. Lett.*, Vol. 13, 774–777, 2014.
15. Yu, A., F. Yang, and A. Elsherbeni, "A dual band circularly polarized ring antenna based on composite right and left handed metamaterials," *Progress In Electromagnetics Research*, Vol. 78, 73–81, 2008.
16. Chaturvedi, D., A. Kumar, and T. Shanmuganantham, "Asymmetric coplanar waveguide-fed CRLH-TL based antenna for WLAN/LTE applications," *International conference on Circuit, Power and Computing Technologies (ICCPCT)*, 1–4, 2015.
17. Rajeshkumar, V. and S. Raghavan, "A compact metamaterial inspired triple band antenna for reconfigurable WLAN/WiMAX applications," *AEU-Int. J. Electron. C.*, Vol. 69, No. 1, 274-80, 2015.
18. Xu, H.-X., G.-M. Wang, Y.-Y. Lv, M.-Q. Qi, X. Gao, and S. Ge, "Multifrequency monopole antennas by loading metamaterial transmission lines with dual-shunt branch circuit," *Progress In Electromagnetics Research*, Vol. 137, 703–725, 2013.
19. Sarkar, D., K. Saurav, and K. V. Srivastava, "Multi-band microstrip-fed slot antenna loaded with split-ring resonator," *Electron. Lett.*, Vol. 50, No. 2, 1498–1500, 2014.
20. Li, X. and J. Tian, "Low-profile fully-printed multi-frequency monopoles loaded with complementary metamaterial transmission line," *Radioengineering*, Vol. 24, No. 1, 64-9, 2015.
21. Bilotti, F., A. Toscano, L. Vegni, K. Aydin, K. B. Alici, and E. Ozbay, "Equivalent-circuit models for the design of metamaterials based on artificial magnetic inclusions," *IEEE Trans. Microw. Theory Techn.*, Vol. 55, No. 12, 2865-73, 2007.